J Mater Sci: Mater Med (2010) 21:1195–1203
DOI 10.1007/s10856-010-3988-6

Nano-scale sliding contact deformation behaviour of enamel under wet and dry conditions

Griselda Guidoni · Michael Swain · Ingomar Jäger

Received: 8 August 2008 / Accepted: 4 January 2010 / Published online: 10 February 2010

Abstract The abrasion response of cross sectional areas of enamel was studied by sliding a rounded diamond conical nano-indenter tip across the surface. The nano-indenter tip (radius ~1,200 nm) was scanned over a specific squared area with a load of 400 μN. Two different environments were chosen: Hank's balanced salt solution (HBSS) and atmospheric laboratory condition. SEM (Scanning Electron Microscopy) and AFM (Atomic Force Microscopy) were used to characterize the final abraded areas. In addition, single scratches with linear incremented load were performed. The normal load and displacement data were utilized in a complementary manner to support the proposed deformation mechanisms. Greater orientation dependence for the case of the single scratches in relation to the abrasion tests was found. The latter results are discussed in terms of plastic deformation effects. The abrasion mechanisms were found to be the same for both wet and dry measurements and similar to that described in a previous study (Guidoni et al., Wear 266:60–68, 2009; Guidoni, Nano-scale mechanical and tribological properties of mineralized tissues. PhD. Montan University Leoben, Leoben, Austria, 2008). However, scratch deformation under fluid measurements shows greater recovery effects and abrasion resistance.

G. Guidoni (✉) · I. Jäger
Department of Materials Physics, University of Leoben, Jahnstr. 12, Leoben 8700, Austria
e-mail: griselda.guidoni@notes.unileoben.ac.at

G. Guidoni
Erich Schmid Institute, Austrian Academy of Sciences, Jahnstr. 12, Leoben 8700, Austria

M. Swain
Biomaterials Science Research Unit, Faculty of Dentistry, University of Sydney, United Dental Hospital, Sydney, Surry Hills, NSW 2010, Australia

M. Swain
Biomaterials Unit, Department of Oral Sciences, School of Dentistry, University of Otago, Dunedin, New Zealand

1 Introduction

Enamel is the outer part of teeth and the highest mineralized tissue in human beings. Loss of hard tooth substance may be caused by factors other than caries and trauma. In modern man the factors contributing to tooth wear are many [1, 2]. Tooth wear can be classified regarding the cause of wear: attrition, abrasion, erosion In particular, in the present work, abrasion will be treated. It is related to pathologic tooth wear caused by friction from a foreign body, independent of occlusion between the teeth. Tooth brushing may be considered an example of this type of wear.

Unlike other calcified human structures, fracture of dental tissue is not self-repairing. One of the most important features of enamel is its good wear resistance, even under severe environmental conditions, such as; wide ranging loads [3], reciprocating grinding-like movements, temperature changes and acidic attacks and/or on the environment chosen for testing [4–7]. Turssi et al. [4] found that over the entire testing period (carried out in a wear simulator after 250000 cycles), the unlubricated condition provided the greatest wear. West et al. [5] studied in vivo and in situ the influence of mean losses of enamel for orange juice, water, experimental blackcurrant juice drink with calcium and blackcurrant juice drink. Even though the wear trends were retained, the absolute values obtained in vivo and in vitro differed considerably, the

latter being higher. In addition, Sarret et al. [7] showed that alcoholic beverages with at least 9 vol% ethanol increased the wear of enamel in comparison with water. On the other hand, saliva is thought to reduce wear [1, 4, 6]. In particular, Li and Zhou [6] concluded that the artificial saliva they used could play both a cooling and lubricant effect during wear process in comparison to their dry measurements.

Abrasion may lead to a loss of essential anatomic form and possibly to a change in masticatory efficiency. Severe abrasion may also expose dentin (the layer below enamel) leading to an acceleration of the loss of hard tissue because of the inferior wear-resistance properties of dentin. Thus, understanding friction and wear behaviour of enamel may help the clinical treatment of teeth and may assist with the development of new dental restorative materials [1, 6, 8, 9].

Wear, among other properties [9], is one of the important considerations taken in choosing the right prosthesis for each particular case. For example, Magne et al. [8] simulated with an artificial mouth masticatory movements and forces and found that depending on the ceramic used the antagonistic healthy tooth became more worn than against normal enamel. Thus, repairing one problem (for example, caries) may lead to another future problem (wear of the opposing healthy teeth).

All the above investigations studied wear mechanism on the micro to millimetre range; however, knowing the inherent hierarchical structure of enamel, understanding wear mechanisms at the nanometre scale may help to elucidate the outstanding performance of enamel even under adverse conditions such as fluidic environments of varying pH, repeated loads, etc. In this respect, incipient research is only just emerging at the nanometre scale. Jandt [10] studied the role of soft drink induced erosion (demineralisation) and remineralisation by means of atomic force microscope (AFM) to measure changes in depth, and with a Berkovich indenter tip measuring changes in hardness. Although less related to wear mechanisms, Habelitz et al. [11] determined the width of the dentine enamel junction (DEJ) by using the different friction coefficients of dentine and enamel while scratching an AFM tip across the interface. A new field of research is now opening regarding the basis of wear behaviour of enamel at the nanometre scale.

To the best knowledge of the authors, tribological studies of enamel at the micrometer scale with the high resolution positioning and testing capabilities a nanoindentation device in combination with an AFM (Atomic Force Microscopy) provide have not been yet reported. In this work, in order to limit the possible influence of environment, we chose to abrade enamel under Hank's balanced salt solution (HBSS) and atmospheric conditions. The latter, plus the scanning of a nano-indenter tip on selected areas of the enamel rod structure, allows us to evaluate the wear process a step further down the hierarchical structure of enamel, i.e. at a scale where mineral fibrils and protein layer responses may be discriminated.

2 Materials and methods

One healthy second premolar extracted for orthodontic reasons from a 12 years old human male together with an incisor of a 1.5 year old steer were examined. Reeh et al. [12] have also investigated both human and bovine enamel macroscopic abrasion and concluded that bovine enamel is a good substitute for human enamel in lubricity studies, reflecting not only the general properties of human enamel lubrication but also the details of oral lubrication regimens. Therefore no further distinction as to the sample origin will be given and all the samples will be treated as enamel.

The samples were cut with a diamond saw in sections along the crown-root direction, carefully avoiding any overheating. One or more pieces of enamel from the same tooth were dehydrated in air ('dry'), the remainder were immersed in Hanks's balanced salt solution, HBSS, ('wet'). An antibacterial was added to HBSS (1/1000 in weight of sodium azide, NaN3, Merck 888). HBSS has been recommended for storage of tooth structure in order to minimize dissolution of the apatite crystallites [13].

The transversal section of the premolar consisting of enamel and dentin was accessible for preparation. The exposed area was ground and polished to a 2500 P grit finish with silicon carbide cloths, followed by polishing in 0.3 μm alumina suspension. In the case of 'wet' conditions, the samples were continuously rinsed with HBSS while polishing, and stored under HBSS at all times to avoid accidental dehydration.

The nano-indenter tip was scanned across the samples using an add-on nano-indentation device (Hysitron Triboscope, Hysitron Inc., Minneapolis, MN, USA) mounted on the scanner head of an AFM stage (Veeco—Digital Instruments, Santa Barbara, CA, USA). Normal load and displacement data can be recorded and stored.

Two types of specimens were evaluated: 'dry', in which the samples were stored and tested under atmospheric conditions, and 'wet', in which samples were stored under HBSS and sample and indenter tip were immersed in HBSS during testing. For both cases a rounded conical diamond indenter tip (nominal radius of $\sim$1,200 nm) was mounted at the end of a tungsten rod ca. 9.5 mm long in order to keep the transducer at a safe distance from the fluid.

The indenter tip was calibrated following the Oliver and Pharr guidelines [14], using a standard fused-quartz probe. The area function was obtained fitting the individual values

at different contact depths with a polynomial function. Typical examples of the maximum penetration depth at 400 μN were obtained by making single point indentation tests under both wet and dry conditions.

2.1 Single scratches

Single scans with linearly increasing loads *on individual enamel rods* were made. The load was linearly increased from 4 μN to a defined maximum load over a distance of ~5 μm at a sliding velocity of 1.2 μm per sec. The maximum loads were 800, 900, 1000, 1200 and 2000 μN for the dry measurements and 400, 1000, 2000 and 4000 μN for the wet measurements. Normal load and displacement were recorded.

2.2 Wear tests

Wear tests were carried out by scanning the diamond indenter tip over a certain micrometer sized square area with 400 μN. In previous experiments [15–17], evidence for removal of material appeared within a reasonable number of scans (i.e. between 1 and 4 full area scans) when using a 400 μN load for both wet and dry experiments. For each test the normal displacement data was recorded. The indenter tip sliding velocity across the specimen is determined by the scanning frequency and the dimension of the scanned area. It varied between 4 and 20 μm/s and it will be individually denoted for each particular test.

Window scan side dimension, scan frequency and number of lines per abraded area were the experimental set up parameters. The indenter tip moves forward a distance equal to the side of the window (single scan) and then comes backwards—at a certain angle—where the next scan begins. The distance between two adjacent scans is given by (size of the window/number of lines). For example, a 2×2 μm^2 made of 128 lines gives a ~16 nm distance between adjacent scans (2000/128). The scans done on the same sliding direction are parallel among themselves. Once one abraded area is completed, in other words, once the set up number of lines per abraded area is done, the subsequent beginning of another test commences where the last abraded area terminated and overlaps with it.

Some tests were deliberately placed inside one single enamel rod and others were chosen to be sufficiently large to incorporate more than one rod, in order to discriminate whether the enamel rod interfaces (or also called sheaths) are influencing the wear behaviour of enamel.

Immediately after some of the wear tests, a control image of 5×5 μm^2 was taken with the nano-indenter tip in the AFM mode at low loads (2–4 μN). In addition, after the wear experiments were completed, some of the abraded areas were imaged with an AFM tip (under atmospheric conditions) and some were viewed with an SEM (under vacuum).

3 Results

The maximum conical tip penetration depth at 400 μN was obtained by making single point indentation tests on the human premolar sample. The penetration data was similar both for wet and dry conditions and it was ~25 nm.

3.1 Single scratches

The *single scratches* generated only deformed surfaces without cracking, even at the maximum loads tested. Figure 1 shows AFM images of scratches in a wet condition. Depth profiles were taken across and along the main scanning direction from higher resolution AFM images. In contrast to the dry state, the scratches with maximum loads of 400 and 1000 μN in the wet condition were not found with the AFM.

For the case of the single scratches, the 2000 μN scratch was made at 180° direction from the 800, 900, 1000 and 1200 μN scratches. The penetration depths of the single scratches done in the same abrasion direction seem to be almost load independent.

The damage depth (d) of single scratch tests done with a rounded conical indenter tip is approximately equal to the measured normal penetration depth (h) [15]. Since the normal penetration depth, h, was continuously measured in situ during the entire length of each scratch test, the normal penetration depth data obtained with the transducer is a direct measurement of the scratch profile, including the elastic and plastic deformation.

The in situ normal penetration depths (h) together with the a posteriori AFM depth profiles of both dry and wet conditions are presented in Figs. 2 and 3, respectively. In all instances, substantial recovery has occurred. For all the conditions, except the scratch to 4000 μN maximum load in the wet condition, the start of a visible imprint with the AFM correlates with a lateral displacement equivalent to a normal applied force between 390 and 490 μN.

3.2 Area scans

For the case of the *area scans*, the normal penetration depth recorded may be used as an in situ measurement of abraded depth [16] following the reasoning for single scratches.

The recorded penetration depths during the entire duration of the last area scan were averaged for each particular test and these values plus their standard deviation are presented in Table 1, in the "displacement data"

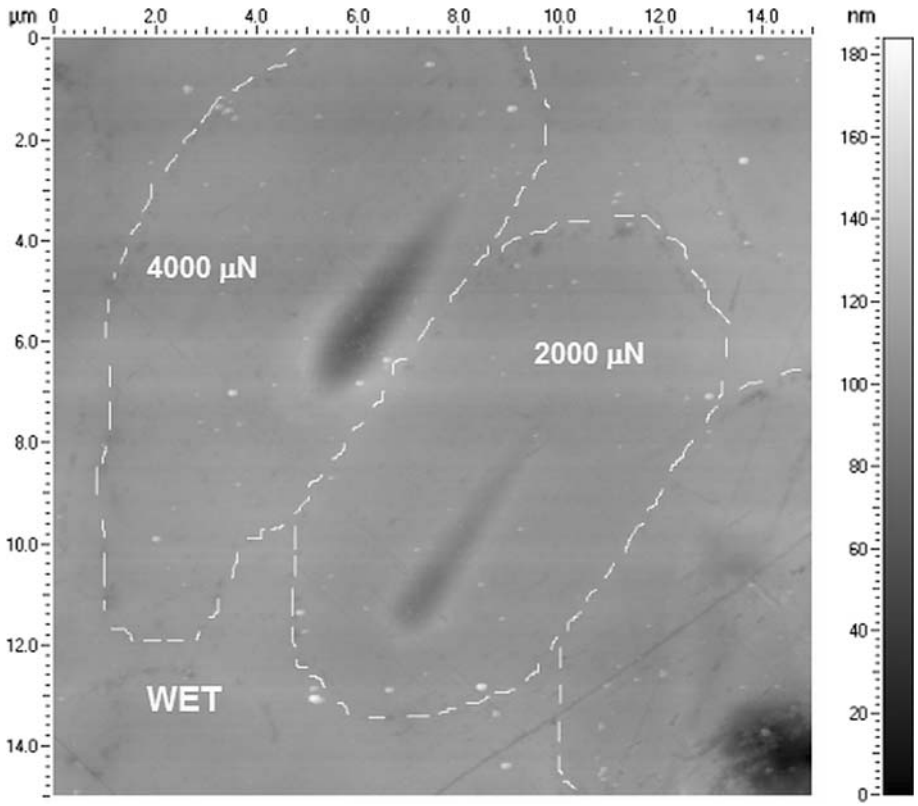

Fig. 1 15×15 µm^2 image of the *wet* single scratches taken with the nanoindenter tip in the AFM mode. The *broken lines* were drawn to show the enamel rod interfaces. Note the proximity of the 4000 µN single scratch to the enamel sheath

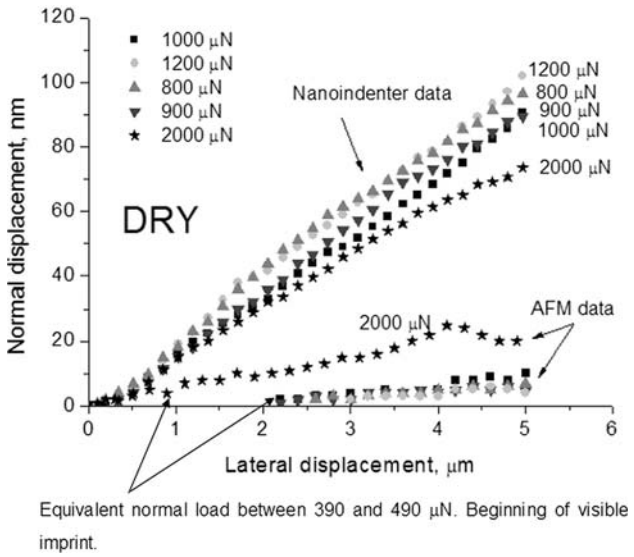

Fig. 2 Normal displacement data versus lateral displacement of the *dry* single scratch tests. "Nanoindenter data" refers to the in situ normal displacement values obtained from the transducer which are equivalent to the damage depth, *d*. "AFM data" was measured after analysing the AFM line profiles along and across the direction of the scratch. The 2000 µN single scratch was done at a 180° change in scanning direction with respect to the remaining single scratches

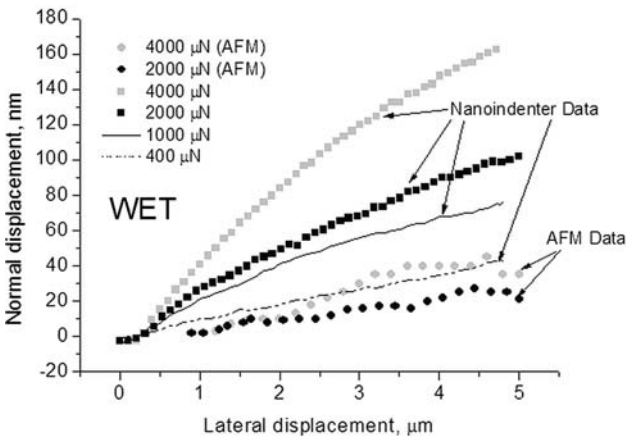

Fig. 3 Normal displacement data versus lateral displacement of the *wet* single scratch tests shown in Fig. 2. "Nanoindenter data" refers to the in situ normal displacement values obtained from the transducer which are equivalent to the damage depth, *d* (*squares* and *lines* in the plot). "AFM data" was measured after analysing the AFM line profiles along and across the direction of the scratch (*circles*). The 400 and 1000 µN were not found with the AFM

column. In addition, the abraded areas were imaged with an AFM tip under atmospheric conditions. Profiles at 10 locations were taken along the slow scanning direction and these ten penetration depths for each single test were averaged and the standard deviation calculated. The latter values are shown in Table 1, in the AFM data column.

Figure 4 shows a low energy mode scanning electron microscopy (SEM) image of an abraded area of the bovine incisor sample (10×10 µm^2, 20 µm/s, 4 area scans,

Table 1 Wear tests carried out at 400 μN in the human premolar sample

	Displacement data (nm)	AFM (nm)
DRY 1	88.6 ± 20.60	82 ± 19
DRY 2	81.9 ± 13.25	87 ± 18
DRY 3	97.5 ± 22.93	81 ± 15
WET 1	54.6 ± 16.28	31 ± 16
WET 2	80.2 ± 6.38	49 ± 15
WET 3	136.7 ± 40.49	–

Seven double scans. 2 × 2 μm^2 areas. The penetration data is shown in nanometres. Each value corresponds to one single test. For the "Displacement data" column, the mean values are the average penetration depth extracted from the corrected normal penetration depth vs. time data throughout the 2 × 2 μm^2 area of the seventh scan follow by their standard deviation. In the case of "AFM" column, mean values are the average depth of 10 profiles taken along the slow scanning direction follow by their standard deviation

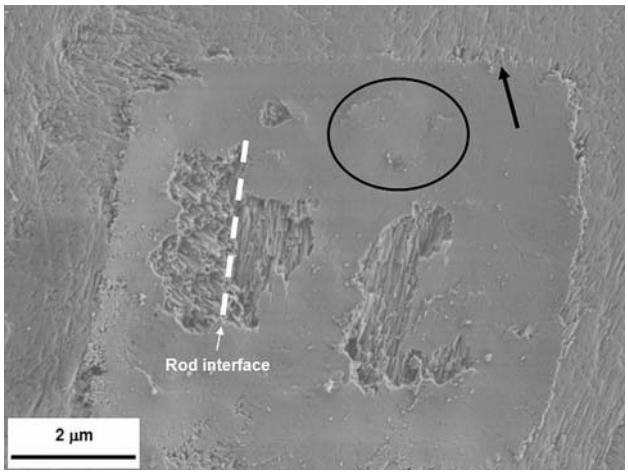

Fig. 4 High resolution SEM image of an abraded area of the bovine incisor sample (10 × 10 μm^2, 20 μm/s, 4 area scans, 400 μN, *wet*) which included more than one rod. The fibrils underneath the removed material can be observed, they are seen to remain intact. Note the different orientation of the fibrils in the abraded area where material was removed (left side removed area), presumably corresponding to a rod interface (marked with a discontinuous *white line*). Compare the smoothness of the abraded area with the outer surface. Moreover, compare the roughness of the fibrils underneath the right side removed area with the right side outer area, judging by this picture they belong to the same rod although only the former region was abraded. The plastically deformed surface is also observed along the borders of the abraded area as a "wave" of material approaching the borders. Marked with an ellipse is an area where incipient delamination is about to occur. The *arrow* indicates a zone where the mineral fibrils seem to be pushed out of the tested area

400 μN, wet). The place were the area scan was done can be clearly seen. More than one enamel rod was deliberately involved during these tests. Certain discontinuous rough areas are present. They correspond to areas were material was removed from the sample while scanning the indenter tip. The extent of material removal was different for regions of adjacent rods, i.e. areas with different fibrils orientation, and within one particular rod. A discontinuous line on the left side of the image was added to show the rod interface between the areas where material was removed. On the right side of the image, the latter mentioned removal situation can be seen. In both cases, the exposed fibrils underneath the removed material can be observed, they seem to remain intact, in other words, they can be discriminated as separate entities.

Two different representative abraded areas are presented in Fig. 5a and b, including their 2D AFM images, line profiles and 3D projections. Figure 5a corresponds to a measurement done in a dry state and Fig. 5b to a wet measurement on the same sample (human premolar sample, 2 × 2 μm^2, 4 μm/s, 7 scan areas, 400 μN). Figure 5a for dry abrasion shows a residual impression approximately 60 nm deep with a very rough surface. Whereas Fig. 5b for wet abrasion, although it has a comparable residual impression, the surface of the impression is smooth. The former suggests a more brittle behaviour in the dry state. In addition, there appears to be pile-up of material on the right hand side, smooth "strips" of material emerging towards the surface are present throughout the whole abraded area (Fig. 5b).

4 Discussion

Comparable single point indentation penetration depths (~25 nm) for both wet and dry conditions and the use of the same indenter tip leads to similar applied contact pressures during the area scan tests (see for instance [18]), while the use of samples of only two different teeth rules out inter-sample scatter. The contact pressure and radius of contact were around 3.8 GPa and 170 nm for both conditions, respectively.

Although most of the literature dealing with mechanical properties of teeth studied human samples [13, 15, 19–24], there are investigations using bovine samples [25–27]. In addition, Reeh et al. [12] clearly showed that bovine enamel may be used as a model for human enamel in salivary lubrication studies. Furthermore, within the scope of the present study, they were found to behave comparatively similar.

It is remarkable that for the case of the single scratches, independent of the test conditions, the corresponding imprint became visible at loads around 400 μN (except for the 4000 μN wet single scratch). In previous studies done under similar experimental conditions [15, 16], this load was found to be a threshold load for observing removal of material after a reasonable number of scans by fatigue damage. In the present study, it also appears to be related to the onset of "plastic" deformation.

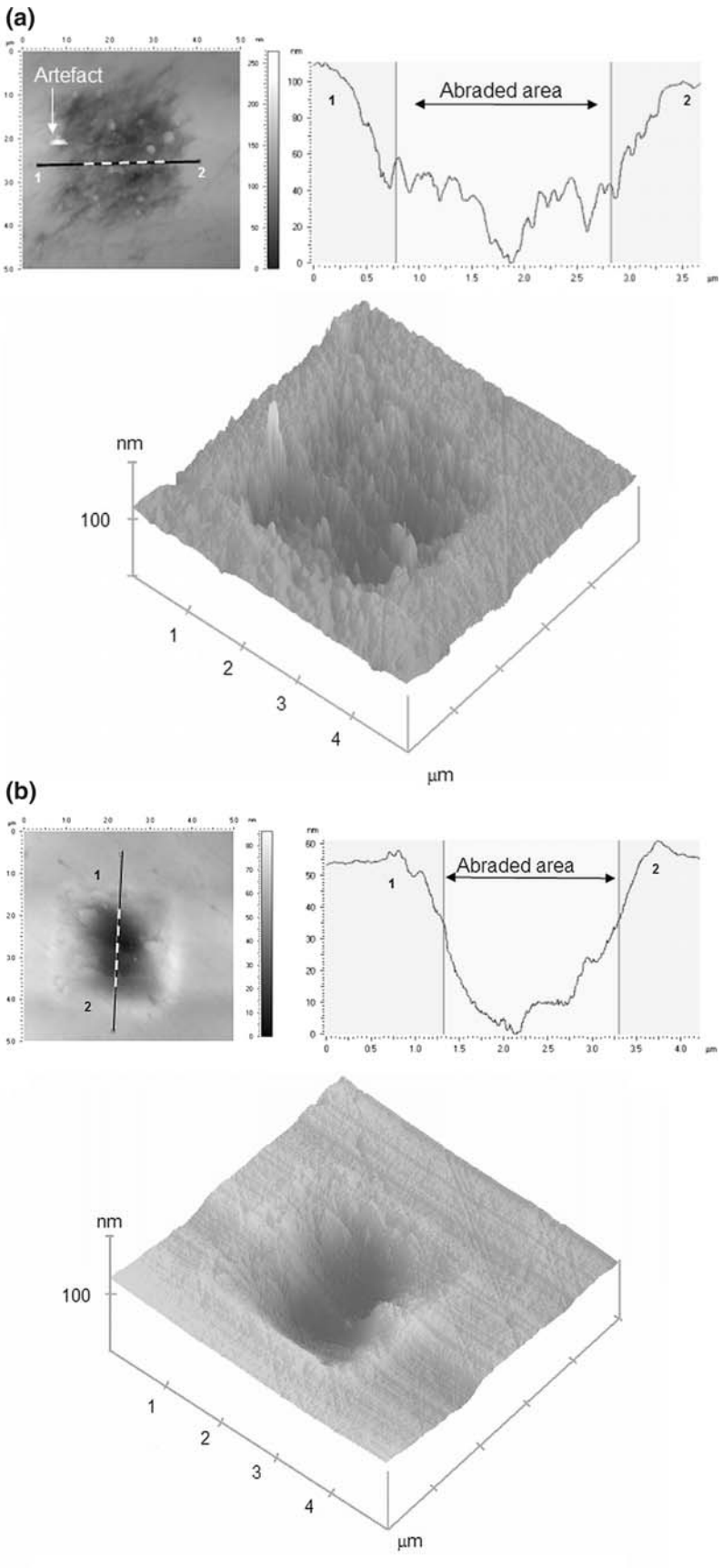

Fig. 5 **a** $5 \times 5\ \mu m^2$ AFM image of an abraded area (human premolar sample, $2 \times 2\ \mu m^2$, 4 µm/s, 7 area scans, 400 µN, *dry*) and its corresponding line profile. Due to an artefact pointed out in the figure the *z*-scale here goes up to 250 nm although the baseline is around 100 nm for the abrasion area. A 3D visualisation from the AFM image is shown in the bottom of the figure. The test was deliberately done inside a rod (rod interfaces not seen in this image). **b** $5 \times 5\ \mu m^2$ AFM image of an abraded area (human premolar sample, $2 \times 2\ \mu m^2$, 4 µm/s, 7 area scans, 400 µN, *wet*) and its corresponding line profile. A 3D visualisation from the AFM image is shown in the bottom of the figure. The test was deliberately done inside a rod (rod interfaces not seen in this image)

The single scratch observations show signs of deformation recovery, as registered after imaging the samples with the AFM facility, in both wet and dry conditions. Even though not a decisive probe, the fact that the low load scratches were not found for the wet sample when AFM imaged, but were for the dry specimen indicate the influence that the environment has on the deformation and recovery processes in enamel.

The 4000 μN single wet scratch was accidentally placed close to the sheath of a rod (Fig. 1). The higher organic content of these regions leads to a different mechanical response with respect to the centre of the rods [22, 28] and as also observed in [15], the sheaths respond different to the cores with respect to abrasion.

Two different scratching responses are found in Fig. 3. The single scratches from 800 to 1200 μN showed higher normal penetration depth than the 2000 μN single scratch, the main difference being a 180° change in scanning direction between the former and the latter tests. The orientation of the fibrils inside the rods is expected to gradually change from one rod to the adjacent one [29] and from the core to the tail of a same rod [30]. Shimizu et al. [31] found by modelling contact deformation of enamel that a change in abrasion direction of 180° may result in a doubling of the tensile stresses just behind the trailing edge of contact between both directions, if the prism angulation is between 45 and 75°. Considering the orientation of the surfaces abraded it is possible that the orientation of the prisms in the chosen area for abrasion was within this limit, which lead to the markedly dependence in abrasion direction of the single scratches tests. Ahead of the indenter the max shear stresses are found if the shear stress trajectories are parallel to the crystallites they will more readily flow than when they are less well aligned.

The abrasion mechanism under the tested dry condition was found to be mainly a plastic asperity deformation process followed by sub-surface fatigue damage, which at a certain combination of load and scan cycles leads to removal of material. The same mechanism describes the abrasion response under the wet conditions tested.

Regarding the abrasion mechanisms, these are clearly evident in Fig. 4. The plastic deformation of the structure not only can be seen from the smoothness of the surface, but also from the remnant "wave" of deformed materials on the borders of the abraded area. The black arrow indicates the place where mineral fibrils appear to be moved by the indenter tip during the abrasion process, although they look to be pushed more than broken. Marked with an ellipse are regions where the sub-surface damage emerged to the surface, similar regions can be seen in Fig. 5b. Those areas will be preferentially removed in further scans, or during cleaning of the sample.

The presence of inter-rod boundaries seems not to influence the abrasion mechanism after successive superimposed scannings, since no trace of them can be found inside the abraded area within the flattened surface layer (Fig. 4), in marked contrast to the results of single scratches. On the other hand, the inter-rod boundary zones are presumably not the loci of preferential damage, since the damage area on the right hand side in Fig. 4 shows no indication of a boundary. In addition, the existence of a removed zone in Fig. 5, where the abraded area was placed inside one single rod also supports this statement.

According to Fig. 5a, the superficial damage generated during the dry measurements seems more likely to be generally lost after the cleaning procedures. Note the smoothness of the outer region in Fig. 5a, when comparing it with the abraded surface even though both surfaces experienced the same cleaning procedure. All the tested areas imaged presented the same feature. On the contrary, for the case of the wet measurement (Fig. 5b) the highly deformed superficial layer seems to be still attached to the substrate after the abrasion tests and cleaning phase. For the dry tests, after the cleaning procedures, the removal of material appears to be related to a general detachment of the superficially deformed layer which also involves taking away material surrounding the abraded area. In Fig. 5a, the size of the damaged area clearly exceeds the 2×2 μm^2 tested area. On the contrary, for the case of the wet samples, removal of material after cleaning, when evident, was highly localized around an already visible damage region and was seldom observed. In general, the wet abraded areas were similar to those shown in Fig. 5b, where the abraded deformed surface is smooth and where the "plastically" deformed structure emerges to the surface. The abraded area without cleaning resembles the final abraded area after cleaning, except for the elimination of debris.

It is notable that the results found for the displacement data and AFM profiles of the abrasion tests in the case of dry measurements are similar, as shown in Table 1, whereas in the wet state they are not. An effective scan size may be considered from the profiles of Fig. 5a and b in which the indenter geometry is taken into account. In the case of the dry sample (Fig. 5a), a 82° semi contact angle is found on the borders of the image by geometric calculations. Considering Hertz equations of elastic constant between two elastic bodies [18], the mentioned angle correlates well with the predicted angle by the equations. On the other hand, for the case of wet condition, there is a 6° increment between the predicted and the measured semi contact angle. The latter observation may also support the better recovery responses under wet than dry conditions.

In addition, although the tests were done on different rods, the dependence on fibril orientation which was found for the single scratch tests could not be found in the case of

the abrasion test. The first scans plastically deform the asperities and its resistance to the deformation will depend on the orientation of the fibrils with respect to the indenter movement. However, once the surface is plastically deformed, further scans will slide on a smooth, highly deformed surface. This smoothing or homogenization effect may explain the fibril orientation and scanning direction dependence for the single scratches and the independence of orientation effects for the abrasion tests.

5 Conclusions

- The abrasion mechanism under the tested dry and wet conditions is mainly a plastic asperity deformation process followed by sub-surface fatigue damage which at a certain combination of load and scan cycles leads to removal of material.
- A load of around 400 μN applied and an associated contact pressure of $\sim$3.8 GPa with this indenter tip appears to be related to the onset of "plastic" deformation of enamel.
- Single scratches are more sensitive to microstructural arrangement than abrasion tests. Once the surface is plastically deformed after the first scans, the following scans will slide on a smooth, highly deformed homogeneous surface. Thus, the microstructural native arrangement, including differences between rod- and inter-rod enamel does not play a role.
- Recovery effects are also present during sliding deformation in enamel for both wet and dry conditions, although the wet HBSS environment favours this behaviour.
- While the highly deformed superficial layer is still visible after the cleaning procedures for the wet sample, it was removed for the dry ones exposing the underlying bulk material. This may indicate a better abrasion resistance for the former than for the latter condition.

Acknowledgements Financial aid through EC Contract No MEST-CT-2004-504465, "Marie Curie Host Fellowships for Early Stage Research Training", is gratefully acknowledged.

References

1. Dahl BL, Carlsson GE, Ekfeldt A. Occlusal wear of teeth and restorative materials. Acta Odontol Scand. 1993;51:299–311.
2. Oh W, DeLong R, Anusavice K. Factors affecting enamel and ceramic wear: a literature review. J Prosthet Dent. 2002;87:451–9.
3. Fernandes CP, Glantz PJ, Svensson SA, Bergmark A. A novel sensor for bite force determinations. Dent Mater. 2003;19:118–26.
4. Turssi CP, Faraoni JJ, Menezes Md, Serra MC. Analysis of potential lubricants for in vitro wear testing. Dent Mater. 2006;22:77–83.
5. West NX, Hughes JA, Parker DM, Newcombe RG, Addy M. Development and evaluation of a low erosive blackcurrant juice drink 2. Comparison with a conventional blackcurrant juice drink and orange juice. J Dent. 1999;27:341–4.
6. Li H, Zhou ZR. Wear behaviour of human teeth in dry and artificial saliva conditions. Wear. 2002;249:980–4.
7. Sarrett DC, Coletti DP, Peluso AR. The effects of alcoholic beverages on composite wear. Dent Mater. 2000;16:62–7.
8. Magne P, Oh WS, Pintado MR, DeLong R. Wear of enamel and veneering ceramics after laboratory and chairside finishing procedures. J Prosthet Dent. 1999;82:669–79.
9. Kelly JR, Nishimura I, Campbell SD. Ceramics in dentistry: historical roots and current perspectives. J Prosthet Dent. 1996;75:18–32.
10. Jandt KD. Probing the future in functional soft drinks on the nanometre scale-towards tooth friendly soft drinks. Trends Food Sci Tech. 2006;17:263–71.
11. Habelitz S, Marshall SJ, Marshall GW Jr, Balooch M. The functional width of the dentino-enamel junction determined by AFM-based nanoscratching. J Struct Biol. 2001;135:294–301.
12. Reeh ES, Douglas WH, Levine MJ. Lubrication of human and bovine enamel compared in an artificial mouth. Arch Oral Biol. 1995;40:1063–72.
13. Habelitz S, Marshall GW Jr, Balooch M, Marshall SJ. Nanoindentation and storage of teeth. J Biomech. 2002;35:995–8.
14. Oliver WC, Pharr GM. An improved technique for determining hardness and elastic modulus using load and displacement sensing indentation experiments. J Mater Res. 1992;7:1564–83.
15. Guidoni G, Swain M, Jäger I. Wear behaviour of enamel at the nano scale with a sharp and blunt indenter tip. Wear. 2009; 266:60–8.
16. Guidoni G, Schöberl T, Dehm G, Jäger I. Abrasion tests on human enamel under wet and dry conditions. The fifth IASTED international conference on Biomedical Engineering "Biomed 2007" 2007; Proceedings of the fifth IASTED International Conference: biomedical engineering 439–45.
17. Guidoni G. Nano-scale mechanical and tribological properties of mineralized tissues. PhD 2008. Montanuniversity Leoben, Leoben, Austria.
18. Johnson KL. Contact mechanics. Series Ninth. Cambridge (UK); 2003.
19. Nalla RK, Balooch M, Ager JW III, Kruzic JJ, Kinney JH, Ritchie RO. Effects of polar solvents on the fracture resistance of dentin: role of water hydration. Acta Biomater. 2005;1:31–43.
20. Cuy JL, Manna AB, Livi KJ, Teaford MF, Weihs TP. Nanoindentation mapping of the mechanical properties of human molar tooth enamel. Arch Oral Biol. 2002;47:281–91.
21. Xu HHK, Smith DT, Jahanmir S, Romberg E, Kelly JR, Thompson VP, et al. Indentation damage and mechanical properties of human enamel and dentin. J Dental Res. 1998;77: 472–80.
22. Ge J, Cui FZ, Wang XM, Feng HL. Property variations in the prism and the organic sheath within enamel by nanoindentation. Biomaterials. 2005;26:3333–9.
23. Guidoni G, Denkmayer J, Schöberl T, Jäger I. Nanoindentation in teeth: the influence of experimental conditions on local mechanical properties. Phil Mag. 2006;86:5705–14.
24. Guidoni G, He LH, Schöberl T, Jäger I, Dehm G, Swain M. Influence of indenter tip geometry and environment on the elastic modulus of enamel. J Mater Res. 2009;24:616–25.
25. Kahler B, Swain MV, Moule A. Fracture-toughening mechanisms responsible for differences in work to fracture of hydrated and dehydrated dentine. J Biomech. 2003;36:229–37.
26. Kitasakoa Y, Burrow MF, Nikaido T, Tagami J. The influence of storage solution on dentin bond durability of resin cement. Dent Mater. 2001;16:1–6.

27. Schilke R, Lisson JA, Bauβ O, Geurtsen W. Comparison of the number and diameter of dentinal tubules in human and bovine dentine by scanning electron microscopic investigation. Arch Oral Biol. 2000;45:355–61.
28. He LH, Swain MV. Energy absorption characterization of human enamel using nanoindentation. J Biomed Mater Res. 2006;A:484–92.
29. Macho GA, Jiang Y, Spears IR. Enamel microstructure—a truly three-dimensional structure. J Hum Evol. 2003;45:81–90.
30. White SN, Luo W, Paine ML, Fong H, Sarikaya M, Snead ML. Biological organization of hydroxyapatite crystallites into a fibrous continuum toughens and controls anisotropy in human enamel. J Dental Res. 2001;80:321–6.
31. Shimizu D, Macho GA, Spears IR. Effect of prism orientation and loading direction on contact stresses in prismatic enamel of primates: implications for interpreting wear patterns. Am J Phys Anthropol. 2005;126:427–34.